

Embryonic Craniofacial Bone Volume and Bone Mineral Density in *Fgfr2*^{+/^{P253R}} and Nonmutant Mice

Christopher J. Percival,¹ Yuan Huang,² Ethylin Wang Jabs,³ Runze Li,² and Joan T. Richtsmeier^{1,*}

Background: Quantifying multiple phenotypic aspects of individual craniofacial bones across early osteogenesis illustrates differences in typical bone growth and maturation and provides a basis for understanding the localized and overall influence of mutations associated with disease. We quantify the typical pattern of bone growth and maturation during early craniofacial osteogenesis and determine how this pattern is modified in *Fgfr2*^{+/^{P253R}} Apert syndrome mice. **Results:** Early differences in typical relative bone density increase are noted between intramembranous and endochondral bones, with endochondral bones normally maturing more quickly during the prenatal period. Several craniofacial bones, including the facial bones of *Fgfr2*^{+/^{P253R}} mice, display lower volumes during the earliest days of osteogenesis and lower relative densities until the perinatal period relative to unaffected littermates. **Conclusions:** Estimates of bone volume and linear measures describing morphology do not necessarily covary, highlighting the value of quantifying multiple facets of gross osteological phenotypes when exploring the influence of a disease causing mutation. Differences in mechanisms of osteogenesis likely underlie differences in intramembranous and endochondral relative density increase. The influence of the FGFR2 P253R mutation on bone volume changes across the prenatal period and again after birth, while its influence on relative bone density is more stable. *Developmental Dynamics* 000:000–000, 2014. © 2013 Wiley Periodicals, Inc.

Key words: micro-computed tomography; bone development; functional regression analysis; Apert syndrome

Key findings:

- Quantifying multiple aspects of gross bone phenotype can provide a more complete understanding of typical bone development and the influence of known mutations.
- Within the mouse skull, endochondrally ossified bones increase in relative density quickly during the prenatal period, while intramembranously ossified bones do not.
- There appear to be shifts in the influence of the FGFR2 P253R mutation on craniofacial bone volume during both the prenatal and postnatal periods.

Submitted 1 August 2013; First Decision 8 October 2013; Accepted 25 October 2013

INTRODUCTION

The skull is morphologically, evolutionarily, and developmentally complex, making the study of normal craniofacial osteogenesis relevant for a large number of research questions. Moreover, an understanding of skull devel-

opment is important for the design of therapeutic agents for the large number of medical syndromes that include craniofacial dysplasias. While the genetic pathways and developmental mechanisms associated with phenotypes such as cleft palate (e.g., Gritli-

Linde, 2008; Dixon et al., 2011; Bush and Jiang, 2012) and craniosynostosis (e.g., Cohen and Maclean, 2000; Morriss-Kay and Wilkie, 2005; Passos-Bueno et al., 2008) have been a focus of research, osteogenesis of whole craniofacial bones is less well understood,

¹Department of Anthropology, Penn State University, University Park, Pennsylvania

²Department of Statistics, Penn State University, University Park, Pennsylvania

³Department of Genetics and Genomic Sciences, Icahn School of Medicine at Mount Sinai, New York, New York

Grant sponsor: NSF; Grant numbers: BCS-1061554; BCS-0725227; Grant sponsor: NIH/NIDCR; Grant numbers: R01DE018500; 3R01DE018500-02S1; R01DE022988.

*Correspondence to: Joan T. Richtsmeier, 409 Carpenter Building, University Park, PA, 16802. E-mail: jta10@psu.edu

DOI: 10.1002/dvdy.24095

Published online 00 Month 2013 in Wiley Online Library (wileyonlinelibrary.com).

particularly in the case of intramembranously ossified bones.

Quantification of normal patterns of craniofacial bone growth and development can provide insight about how differences in cellular origin, mode of ossification, and initial timing of ossification may be associated with variation of skull phenotypes. In addition, quantifying how mutations associated with craniofacial dysmorphology change these baseline patterns of growth and development can help reveal how mutations lead to changes in skeletal phenotype through dysregulation of developmental systems, thereby contributing to the development of therapeutic treatment. Landmark based morphometrics has become a standard way to quantify important changes in gross bone morphology across the skull that are based in known mutations associated with human syndromes (e.g., Olson et al., 2004; Perlyn et al., 2006; Hill et al., 2007; Boughner et al., 2008; Hallgrímsson et al., 2009; Martínez-Abadías et al., 2010; Schmidt et al., 2010; Percival et al., 2012) and to identify locations for targeting specific sites for cellular analyses (Martínez-Abadías et al., 2013). Landmark-based measures estimate important aspects of craniofacial bone phenotype. However, the quantification of additional facets of skull phenotype, including bone volume and density, can provide additional complementary data on the nature of skeletal variation and can serve as the basis for additional nuanced hypotheses about the origins of normal and syndromic skeletal variation.

In this study, we quantify important aspects of pre- and perinatal growth and maturation for individual craniofa-

cial bones, and then determine how this pattern is modified by the Apert syndrome associated *Fgfr2* P253R mutation. Here, growth refers to changes in bone quantity while maturation refers to changes in bone quality over development. Previous analysis of *Fgfr2*^{+ / P253R} Apert syndrome mice indicated that mutants can be identified as early as embryonic day (E) 16.5 by their relatively domed heads (Yin et al., 2008), that coronal fusion is evident along with changes in cell activity during the fetal period and that skull size is smaller at birth (Holmes et al., 2009; Wang et al., 2010; Martínez-Abadías et al., 2010). Both intramembranous and endochondral ossification processes are known to be influenced by the P253R mutation (Yin et al., 2008; Wang et al., 2010) and although dysmorphology may be more apparent in the facial skeleton, dysmorphology appears elsewhere in the skull of *Fgfr2*^{+ / P253R} mice (Martínez-Abadías et al., 2010; Du et al., 2010). Therefore, we hypothesize that all individual craniofacial bones of *Fgfr2*^{+ / P253R} mice will display reduced bone volume and relative bone mineral density from the time of initial ossification through the postnatal period, although bones previously associated with early suture fusion (frontal and parietal bones) and those with known shape changes (maxilla, premaxilla, palatine, nasals) are expected to display more severe reductions.

EXPERIMENTAL PROCEDURES

Sample and Imaging

We use the previously described Apert syndrome *Fgfr2*^{+ / P253R} mouse model in this study (Wang et al., 2010). *Fgfr2*^{+ / P253Rneo} mice were crossed with

EIIA Cre homozygotes so that roughly half of our litters heterozygously express the *Fgfr2* P253R mutation in all tissues (*Fgfr2*^{+ / P253R}) and half do not express this mutation (*Fgfr2*^{+ / +}). Based upon timed mating and evidence of pregnancy, litters were sacrificed on embryonic days (E) 14.5, 15.5, 16.5, 17.5 and postnatal days (P) 0 and 2. The E17.5, P0, and P2 mice in this study were used in previous landmark based morphometric analyses (Wang et al., 2010; Martínez-Abadías et al., 2010; Motch et al., 2012; Hill et al., 2013). After sacrifice, specimens were fixed in 4% paraformaldehyde and stored in 0.01 M phosphate buffered saline with sodium azide as an antibacterial agent. Care and use of mice for this study were in compliance with relevant animal welfare guidelines approved by Mount Sinai School of Medicine and Pennsylvania State University Animal Care and Use Committees.

High resolution micro-computed tomography (μ CT) images of mouse heads (Table 1) were acquired in air at the Center for Quantitative X-Ray Imaging at Pennsylvania State University (www.cqi.psu.edu) using an OMNI-X Universal HD600 industrial x-ray computed tomography system (Varian Medical Systems, Palo Alto CA). Solid hydroxyapatite phantoms (QRM GmbH, Möhrendorf, Germany) scanned with each set of skulls allowed us to linearly associate relative x-ray attenuation values with bone mineral density estimates.

Bone Volume and Density Histograms

Using Avizo software (Visualization Sciences Group, Burlington, MA),

TABLE 1. Sample Sizes of *Fgfr2*^{+ / P253R} and *Fgfr2*^{+ / +} Mice, the Associated Image Resolution, the Minimum, and μ CT Scan Settings by Age

Age	No. of <i>Fgfr2</i> ^{+ / +} specimens	No. of <i>Fgfr2</i> ^{+ / P253R} specimens	Voxel width (mm)	Slice thickness (mm)	kVp	mA	Frame averaging	No. of projections
E15.5	7	7	0.0107	0.0125	100	0.19	5	2,400
E16.5	16	9	0.0107	0.0125	100	0.19	5	2,400
E17.5	7	9	0.0137	0.0154	110	0.18	3	2,400
P0	14	11	0.0151	0.0159	130	0.15	4	1,440
P2	8	5	0.0151	0.0159	130	0.15	4	1,440

craniofacial bones with a minimum of 74.0 mg/mm³ partial density of hydroxyapatite were manually identified (segmented) from μ CT images of E15.5, E16.5, and E17.5 skulls (no bone was detected in the μ CT images of E14.5 specimens). Manual segmentation minimizes segmentation error associated with the relatively low levels of ossification within embryonic bones. Craniofacial bones of the larger and more highly ossified P0 and P2 specimens were segmented using a modified version of a previously described semi-automatic segmentation method (Percival et al., 2012). After segmentation of specimens of all ages, a histogram of 126 bone density values between 74.0 and 372.2 mg/mm³ partial density of hydroxyapatite (Fig. 1) was estimated for each identified bone. Because of image saturation for some bones of the older specimens, the highest density values may include volumes of bone above the maximum density value.

Measurements from 16 bones serve as the basis of our analysis (Fig. 2). For each age-genotype associated group of mice, either the right or left version of bilateral bones (shown previously to display similar measures within individuals; Percival, 2013) was chosen for analysis based on segmentation accuracy. Teeth were not segmented during manual segmentation of embryonic specimens to avoid confounding them with surrounding bone. For older specimens, teeth were manually segmented independently and their density histograms were subtracted from associated bone density histograms before analysis.

Total individual bone volumes, the sum of histogram values for all densities multiplied by the μ CT image resolution, were compared between the genotypes within age categories with two-sample Wilcoxon (Mann-Whitney) tests ($\alpha = 0.05$), including Bonferroni correction for multiple testing, using R (R Developmental Core Team, 2008). Mean total bone volumes, calculated for each age-genotype combination, serve as a proxy for bone size, while differences in volume between ages represent bone growth. Mean individual bone volumes standardized by the total bone volume of the 16 bones under

study represent relative bone size at each age-genotype combination.

Standardized bone density histograms were calculated for each specimen by dividing each entry of the voxel count filled bone density histograms by the total number of voxels associated with that bone. This standardizes voxel counts by total bone volume, removing variation associated with differences in scale. Mean standardized bone density histograms were calculated for the bones of each age-genotype combination. Spline curves approximating these standardized histograms, called relative density curves, serve as the basis for subsequent density analysis (Fig. 1) and provide the basis for the quantitative evaluation of bone maturation.

Using the *Fgfr2*^{+/+} relative bone density curves as a comparative, normative bone maturation baseline, functional regression analysis was performed with the *fda* package in R (Ramsay et al., 2009), to determine the influence of the P253R mutation on bone maturation across the earliest stages of craniofacial ossification. Because image saturation in some bones of the older specimens has a strong artificial influence on functions estimated from histograms, the five highest bone density values were not included in functional analysis. Using the remaining 121 values from the standardized histograms, cubic spline functions were estimated for each bone using five knots. Functional multivariate regressions were computed across density values (d) for each bone with *Age* as a numerical covariate, *Genotype* as a binary covariate, and with an optional *Age*Genotype* interaction term using the following model:

$$E(y_i(d)) = \beta_0(d) + \beta_1(d) \textit{Genotype} + \beta_2(d) \textit{Age}$$

$$E(y_i(d)) = \beta_0(d) + \beta_1(d) \textit{Genotype} + \beta_2(d) \textit{Age} + \beta_3(d) \textit{Int}_{\textit{Genotype, Age}}$$

Three separate multivariate regressions of relative density curves (using all ages, only prenatal ages [E15.5–P0], or only postnatal ages [P0, P2]) were computed for each bone to identify differences in the effects of the P253R mutation before and after birth. For each bone,

regressions were estimated only for those age classes in which the bone could be measured in all specimens. The 95% confidence intervals of the resulting coefficient curves were computed to determine the statistical significance of the effect of the associated covariate.

RESULTS

Volume Analysis

Ossified portions of some of the 16 bones identified from μ CT images display gross differences in extent and shape between *Fgfr2*^{+/P253R} Apert model mice and their unaffected littermates (*Fgfr2*^{+/+}) (Fig. 2). The ossified volume of the skull increases every day between E15.5 and postnatal day P2 (Table 2), with no significant difference in overall bone volume between the genotypes at any age. The proportional mean volume of individual elements varies between ages (Table 2). Further illustrations of bone extent and volume are available at www.getahead.psu.edu/ApertDevVol for interested readers.

The volumes of specific elements differ between genotypes at some ages, suggesting strong trends (Figs. 3, 4). At E15.5, *Fgfr2*^{+/P253R} mice display (nonsignificant) lower mean volumes than *Fgfr2*^{+/+} mice across all relatively well-ossified bones (Fig. 3A). Importantly, removing a single *Fgfr2*^{+/P253R} mouse of particularly high ossification from the sample changes to significant the differences in volumes of SquT, Max, and PMax between *Fgfr2*^{+/+} and *Fgfr2*^{+/P253R} mice, revealing the effects of strong intra-group variation on analytical results. The bones of E16.5 *Fgfr2*^{+/P253R} mice have lower or similar mean volumes relative to *Fgfr2*^{+/+} (Fig. 3B). At E17.5, bone volumes are not significantly different between the genotypes (Fig. 3C). P0 *Fgfr2*^{+/P253R} mice display higher mean volumes than *Fgfr2*^{+/+} for some bones and lower for others (Fig. 4A). At P2, the volumes of six bones are significantly reduced in *Fgfr2*^{+/P253R} mice (Fig. 4B). Because of relatively high levels of semi-automatic segmentation error for Pal, PSph, SphA, and SphB in P2 mutants, the results for these bones

TABLE 2. Comparison of Patterns of Bone Growth Between Genotypes^a

	<i>Fgfr2^{+/+}</i>					<i>Fgfr2^{+ / P253R}</i>				
	Mean total bone volume (mm ³) by age, with standard deviation									
	E15.5	E16.5	E17.5	P0	P2	E15.5	E16.5	E17.5	P0	P2
	0.28 (0.11)	1.23 (0.29)	3.11 (0.48)	5.44 (1.05)	10.89 (1.96)	0.20 (0.17)	1.05 (0.35)	3.62 (0.45)	5.58 (1.42)	9.99 (2.15)
	Mean % of total volume at each age (SD)									
	E15.5	E16.5	E17.5	P0	P2	E15.5	E16.5	E17.5	P0	P2
Man	53.3 (8.8)	35.7 (3.4)	31.2 (1.6)	26.8 (1.4)	22.2 (1.0)	54.1 (9.0)	31.7 (1.1)	28.6 (1.3)	24.8 (1.2)	23.7 (1.0)
BasO	12.3 (4.4)	13.8 (1.1)	10.9 (0.9)	10.7 (0.9)	7.5 (0.4)	12.6 (3.1)	17.0 (0.8)	11.8 (0.7)	11.0 (1.4)	7.9 (0.8)
Fro	10.3 (3.4)	12.6 (0.8)	12.9 (0.6)	10.3 (0.7)	10.7 (0.4)	14.1 (1.7)	13.1 (0.9)	12.9 (0.7)	10.1 (0.5)	10.6 (0.4)
Max	11.5 (1.7)	11.1 (0.6)	11.6 (0.7)	10.0 (0.5)	9.6 (0.1)	8.3 (1.5)	9.7 (0.4)	12.7 (0.8)	12.2 (0.6)	10.8 (1.3)
LatO	4.9 (2.4)	8.4 (1.0)	7.0 (0.8)	6.6 (0.6)	4.7 (0.2)	5.1 (3.5)	10.2 (0.6)	7.5 (0.6)	6.9 (0.9)	4.8 (0.2)
PMax	2.4 (1.2)	3.5 (0.5)	4.3 (0.9)	5.5 (0.7)	5.9 (0.2)	1.0 (0.8)	2.1 (0.5)	4.1 (0.8)	6.0 (0.6)	5.8 (0.9)
Pal	2.8 (0.6)	3.3 (0.2)	3.6 (0.2)	3.9 (0.3)	3.2 (0.2)	2.4 (0.5)	3.7 (0.4)	4.2 (0.3)	4.4 (0.3)	4.0 (0.2)
Par	1.1 (0.9)	4.3 (0.9)	5.9 (1.2)	4.7 (1.0)	6.5 (0.4)	1.6 (1.7)	5.1 (0.8)	6.2 (0.7)	4.6 (1.0)	5.9 (0.4)
SquT	0.8 (0.1)	1.5 (0.2)	2.2 (0.1)	2.8 (0.4)	3.0 (0.1)	0.5 (0.2)	1.1 (0.1)	2.0 (0.2)	2.6 (0.2)	2.8 (0.1)
SphB	0.3 (0.3)	3.0 (0.8)	4.7 (0.4)	6.0 (0.6)	5.2 (0.3)	0	3.5 (0.5)	4.5 (0.3)	5.8 (0.7)	4.8 (0.3)
SphA	0.3 (0.3)	1.7 (0.4)	2.9 (0.2)	3.6 (0.6)	3.3 (0.2)	0.4 (0.2)	1.9 (0.3)	2.8 (0.2)	3.7 (0.2)	3.2 (0.2)
IPar	0	0.6 (0.3)	1.8 (0.5)	2.0 (0.7)	3.8 (0.2)	0	0.6 (0.2)	1.5 (0.2)	1.6 (0.5)	3.0 (0.3)
PetT	0.1 (0.1)	0.5 (0.2)	0.5 (0.1)	1.1 (0.2)	5.3 (1.7)	0	0.3 (0.1)	0.4 (0.1)	0.9 (0.2)	3.7 (0.7)
SquO	0	0	0	3.3 (0.5)	4.3 (0.3)	0	0	0	2.0 (1.0)	3.6 (0.5)
PSph	0	0	0.2 (0.1)	2.4 (0.3)	3.1 (0.2)	0	0	0.4 (0.2)	2.6 (0.4)	3.7 (0.2)
Nas	0	0	0.2 (0.1)	0.6 (0.3)	1.6 (0.1)	0	0	0.4 (0.2)	0.7 (0.6)	1.7 (0.4)

^aAbove are mean total volumes of the 16 bones under study by age measured as mm³, with standard deviation in parentheses. Below is the mean relative volume of each bone by age and genotype, calculated as the percentage of mean total bone volume at the associated age, with standard deviation in parentheses. Bone abbreviations are defined in Figure 2. A graphical illustration of this table can be found at www.getahead.psu.edu/ApertDenVol by interested readers.

at P2 and in the postnatal regression should be accepted with caution.

Histogram Analysis

Bone density histograms summing all density values within identified bones were standardized by total bone volume to serve as a basis for comparing relative bone densities across specimens. Functional representations of these standardized bone density histograms, called relative density curves, were used as the basis of statistical comparisons of relative bone density (Fig. 1). Relative density curves of *Fgfr2^{+/+}* mice, representing each age of a given bone, were plotted together to illustrate typical changes in relative bone mineral density. Most bones display very low relative density at E15.5, but mature in one of three ways (Fig. 5; Table 3). Group 1 (continuous increase) bones display a consistent and continuous change from low relative bone density to higher density

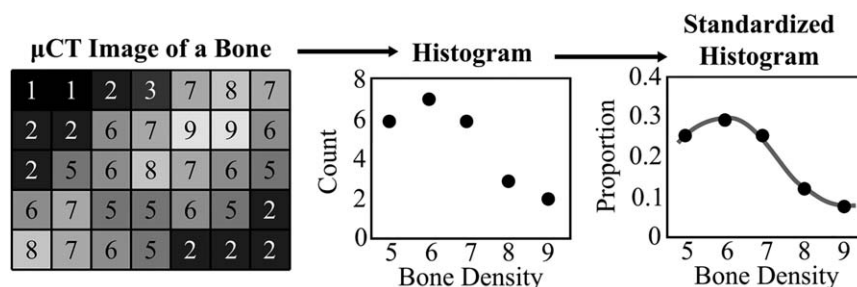


Fig. 1. Simplified example illustrating relative density histogram and curve quantification; where minimum bone density is 5 and the count of bone voxels is 24. Bone volume = 24 * μ CT image resolution. Standardized Histogram = Histogram / 24. Relative density curves are estimated from standardized histograms using cubic spline functions.

across the age range (Fig. 5A,B). Group 2 bones (medium density) display an intermediate relative bone density from E16.5 to P2 (Fig. 5C–E). Group 3 bones (low density) retain a low relative bone mineral density until the postnatal period, when increase in relative density often occurs between P0 and P2 (Fig. 5F–H). A strong increase between P0 and P2 is particu-

larly apparent for bones of group 3, but not limited to this group. Illustrations of relative density curves for all skull bones are available at www.getahead.psu.edu/ApertDenVol for interested readers.

Functional multivariate regressions of relative density curves for each specimen indicated that *Age* and *Genotype* are significant factors in

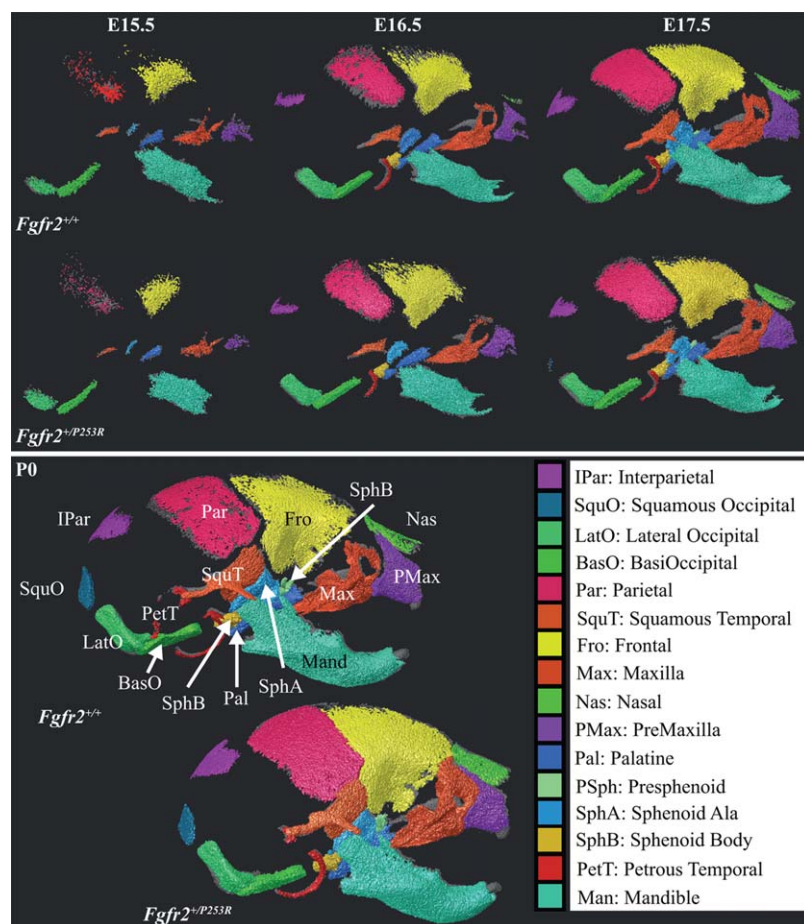


Fig. 2. Analysis of bones identified from the right lateral view of μ CT images of representative specimens at embryonic day (E) 15.5, E16.5, E17.5, and postnatal day (P) 0 for both genotypes. Bones being analyzed are brightly colored, while the rest of the skull is transparent gray. There are some noticeable differences in individual bone shape and extent between the genotypes at each age. Bones are identified by name and abbreviation on the $Fgfr2^{+/+}$ P0 specimen. The rostral aspect of the skulls is to the right and the dorsal aspect is toward the top of the page. Images are not to scale. Higher resolution images displaying bone extent for all ages from right lateral and ventral views are available at www.getahead.psu.edu/ApertDenVol for interested readers.

influencing relative bone density. The addition of an interaction term between *Age* and *Genotype* in the regressions did not qualitatively change the results, so we report the results of the regressions without the interaction term. Most bones show a significant age effect for which the proportion of low density bone strongly decreases with age and the proportion of higher density bone increases with age more subtly (Figs. 6, 7). The bones that display weak or nonsignificant age effects are IPar, Man (Fig. 6D), PetT, and Max for the prenatal regression (E15.5–P0), and LatO (Fig. 7C) for the postnatal regression (P0–P2). Bones that typically display more obvious changes in relative density curves

across the ages and proportionally more high density bone (Fig. 5) also tend to have age effect coefficients that remain significant across a wider range of density values (Figs. 6, 7).

In all cases of a significant effect of *Genotype* on relative bone density, the FGFR2 P253R mutation is associated with a higher proportion of low density bone and a lower proportion of higher density bone, which is similar to a reduction in the value of the *Age* covariate. For prenatal regressions, genotype has a significant effect for Man (Fig. 6D), Max, SquT (Fig. 6A), and PMax, while PetT and Pal display a weakly significant genotype effect. For postnatal regressions, genotype has a significant effect on Max, SquT, Pal, and a weak effect on Man (Fig.

7D), Fro (Fig. 7B), PetT, and SquO. For bones that display a significant genotype effect, the relative density curves of $Fgfr2^{+/P253R}$ mice tend to cluster separately from the $Fgfr2^{+/+}$ mice for all ages. This contrasts with bone volumes that show inconsistent differences between $Fgfr2^{+/P253R}$ and $Fgfr2^{+/+}$ across the ages (Figs. 3, 4).

DISCUSSION

Bone Volume and Relative Density Quantification

We have delineated a method that takes advantage of the properties of μ CT to provide novel measurements of bone growth and maturation across the earliest periods of craniofacial ossification, filling a void left by more traditional approaches. μ CT provides direct 3D representations of ossified volumes, allowing quantification of their shape, size, relative density, and spatial association. The variation in measures noted between specimens of the same genotype is typical of quantitative analyses of unsealed phenotypes in mouse models (e.g., Hill et al., 2007; Boughner et al., 2008).

Measurements of bone volume and density based on phantom-calibrated μ CT images are likely to be lower than values produced by other methods, including whole-mount staining and histology. This is due to comparatively lower spatial resolution of μ CT and because mineralized tissue is identified in μ CT images rather than initial collagen or calcium deposits or expression of other early bone markers visualized with some staining techniques.

Normal Craniofacial Bone Maturation and Growth

Our estimates of “typical” bone density, based on unaffected littermates, vary considerably within litters and may be specific to the C57BL/6 background (Beamer et al., 1996, 2001). Improvements in identifying the relative developmental age of the embryonic craniofacial complex, as done for limb buds (Boehm et al., 2011), may enable more precise age-phenotype associations.

Ontogenetic changes revealed in mean relative density curves of $Fgfr2^{+/+}$ mice serve as a proxy for

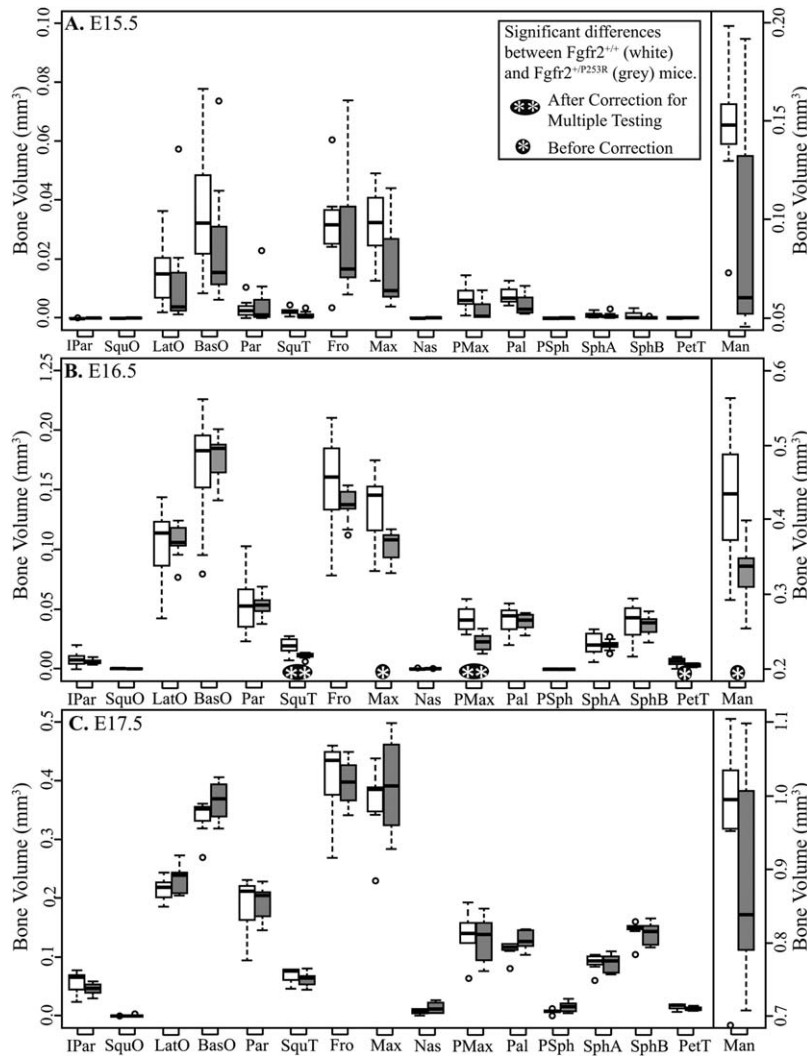


Fig. 3. Boxplots of bone volumes by age, comparing the bone volume distributions for each bone between both genotypes at (A) embryonic day (E) 15.5, (B) E16.5, and (C) E17.5. White boxes represent *Fgfr2*^{+/+} and grey boxes represent *Fgfr2*^{+/P253R}. Dots represent outlier values that are more than 1.5 times the interquartile range from the box. Bone abbreviations are defined in Fig 2.

normative bone maturation trajectories. Qualitative comparisons of these curves revealed three patterns of maturation. All cranial bones in group 1 (Fig. 5A,B) ossify endochondrally and display an increase in relative bone density for each age interval from initial ossification until P2, as well as a peak in their curves at later ages. Significant age coefficients from prenatal, but not necessarily postnatal, multivariate regressions of early ossifying members of group 1 match this interpretation. Ossification within a cartilage model appears to promote a quick increase in relative bone density after initial ossification, although the pace of density increase may slow after birth.

Group 2 and 3 bones maintain a stable level of relative bone density even as their volumes increase during the earliest ages of ossification (Figs. 3, 4). The intramembranous bones of group 2 (Fig. 5C–E) sustain weakly convex curves between E16.5 and P0 or P2, which represent moderate relative bone density without much increase. Group 3 bones (Fig. 5F–H), which tend to ossify in the more peripheral regions of the skull, retain a steep convex curve of relatively low density until an increase between P0 and P2. PetT is the exception, having a more central location in the cranial base but retaining low density prenatally.

Fundamental differences between intramembranous and endochondral

osteogenesis may account for increased relative density of most endochondral bones during the embryonic period and moderate or low relative density of intramembranous bones before postnatal density increases. Cartilage models of endochondral bones roughly reflect the shapes of associated adult bones (Eames and Schneider, 2008). Intramembranous ossification requires sustained proliferation of precursor cells within mesenchymal condensations that do not resemble their ossified versions until after ossification has already begun within the condensations (Lana-Elola et al., 2007; Yoshida et al., 2008). Perhaps this early proliferation of mesenchyme precursors occurs at the expense of higher densities of differentiating osteoblasts within intramembranous bones during the earliest stages of ossification.

The PetT may represent an important exception to the idea that endochondral bones mature more quickly during initial ossification. The PetT exists primarily as a relatively small ossified annulus for much of the embryonic period until a swift and substantial increase in PetT volume occurs between P0 and P2 (Table 2). In this way, it may be similar to SquO and PSph, which do not ossify until later in development, but mature very quickly once initiated. If the annulus is disregarded from our measurement of the PetT, because its developmental origin is distinct from the rest of the bone (Kardong, 2012), it is possible that the curves of PetT would fall in group 1, particularly if measurements after P2 were available.

Effect of the P253R Mutation on Bone Growth

We reject our hypothesis that all individual craniofacial bones of *Fgfr2*^{+/P253R} mice display reduced bone volume and relative bone mineral density from initial ossification into the postnatal period. Instead, certain bones are significantly reduced while others are not. In addition, the influence of the P253R mutation on bone volume changes across the prenatal period and then again postnatally, while the influence of genotype on relative density curves of each bone is stable across ages. These differences in volume and relative

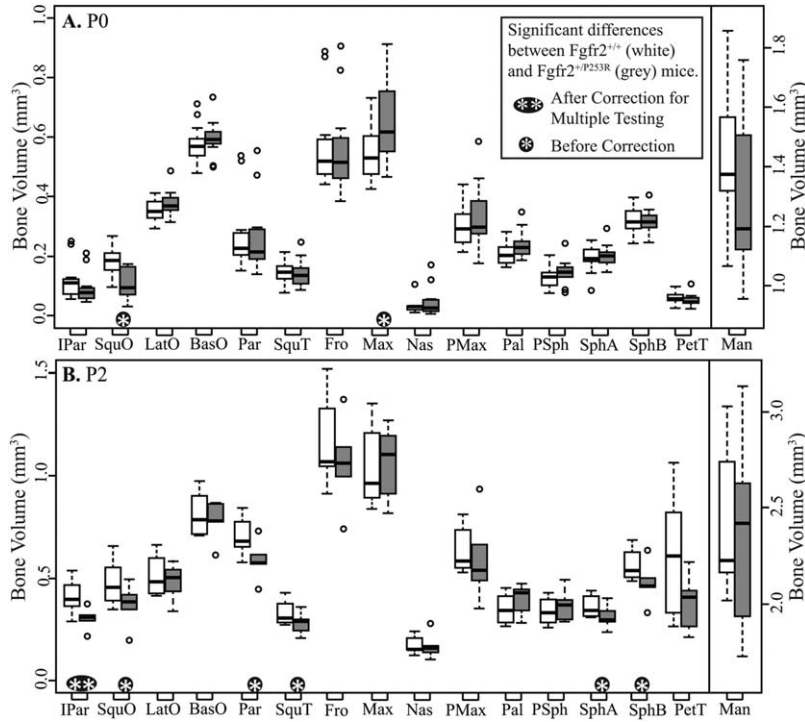


Fig. 4. Boxplots of bone volumes by age, comparing the bone volume distributions for each bone between both genotypes at (A) postnatal day (P) 0 and (B) P2. White boxes represent $Fgfr2^{+/+}$ and gray boxes represent $Fgfr2^{+/P253R}$. Dots represent outlier values that are more than 1.5 times the interquartile range from the box. Bone abbreviations are defined in Fig 2.

density suggest more nuanced hypotheses about the bases of craniofacial dysmorphology in these mice and in humans with Apert syndrome.

Below, we discuss the implications of our results and compare them with the results of other studies. Differences in background strain may account for some of the differences between the results of our study and that of others. Direct comparisons between our whole bone measures and those stemming from landmark based morphometrics or cranial suture based histology may not always be appropriate. We attempt to be explicit about differences in the data on which the cited results are based throughout the discussion.

Prenatal Effect

Most cranial bones of $Fgfr2^{+/P253R}$ mice display lower mean volumes at E15.5 relative to unaffected littermates (not statistically significant), while several display significantly lower volumes at E16.5. These same bones appear reduced in ossified extent within μ CT images at these ages (Fig. 2). These

reductions in whole bone volume appear to disagree with observations made at the coronal suture of different Apert syndrome model mice, where increased osteoid deposition at approximating bone fronts are observed by E15.5 or E16.5 (Holmes et al., 2009). The potential reasons for these conflicting results include: differences between the two Apert mouse models; acute and specific dysregulation at the coronal suture; and/or the fact that μ CT images display relatively well ossified bone as opposed to the osteoid and collagen deposition typically visualized by cell biology techniques.

Similar volumes across genotypes for most bones at E17.5 suggest a period of volume catch-up for $Fgfr2^{+/P253R}$ mice before E17.5. Continued increase leads to larger mean volumes for some bones in P0 $Fgfr2^{+/P253R}$ mice, including Max. Although the effect of the P253R mutation on individual bone volume varies across prenatal ages, facial bones and PetT of $Fgfr2^{+/P253R}$ mice that display significantly lower volume at E16.5 also display lower relative density across the prenatal period. This sug-

TABLE 3. Groups of Bones Defined by the Pattern of Change of Their Relative Density Curves Between E15.5 and P2 for $Fgfr2^{+/+}$ Mice^a

Group 1 – Continuous Increase	Group 2 – Moderate Density	Group 3 – Low Density
BasO	Fro	IPar
LatO	Pal	Par
SphB	Max	PetT
SquO	Man	Nas
PSph	SquT	PMax
	SphA	

^aBone abbreviations are defined in Figure 2.

gests that the P253R mutation retards bone maturation starting at initial ossification and that relative density remains reduced even as bone volumes approach or exceed normal levels.

Previous histological observations of the influence of the P253R mutation on local cell activity near cranial sutures may provide a partial explanation for the catch-up in bone volume observed for some bones by E17.5 and P0. Proliferation at the osteogenic fronts of the coronal sutures of $Fgfr2^{+/S252W}$ mice was reduced significantly at E16.5, although it did not differ at E13.5 or E15.5 (Holmes et al., 2009). Proliferation was also reduced at E17.5 at the coronal sutures of $Fgfr2^{+/P253R}$ mice, but not at E19 or P5 (Wang et al., 2010). Concurrent with reduced proliferation, increased osteoblast differentiation was noted at the coronal sutures in $Fgfr2^{+/P253R}$ mice between E16.5 and E17.5 (Yin et al., 2008) and between E17.5 and P5 (Wang et al., 2010). Decreased proliferation of preosteoblastic cells and increased differentiation associated with the P253R mutation may coincide with known shifts in *FGFR* expression during osteoblast maturation (Morriss-Kay and Wilkie, 2005) and/or the switch from an expanding population of mesenchymal progenitors to the more typically described ossification front moving outward from intramembranous bone ossification centers (Lana-Elola et al., 2007; Yoshida et al., 2008).

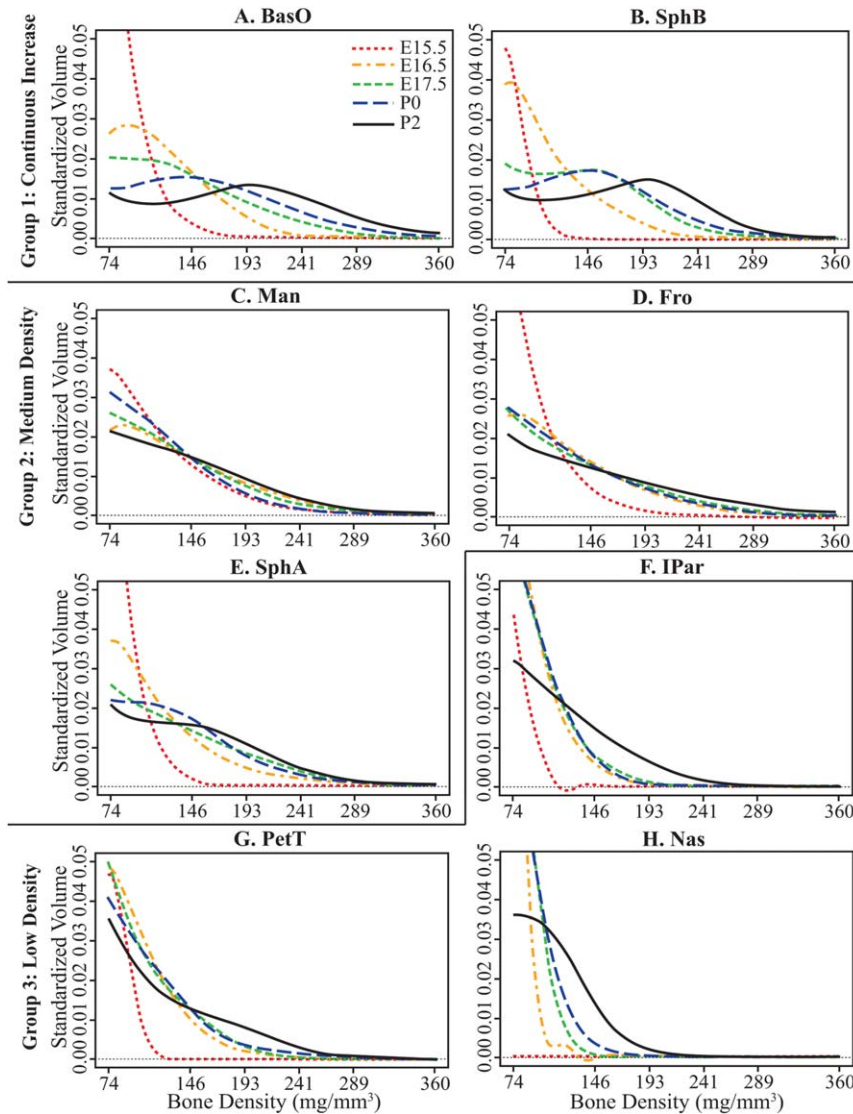


Fig. 5. A–H: Mean relative bone density curves for a subset of bones of *Fgfr2*^{+/+} specimens at each age, representing three patterns of bone maturation. The axis scales are standardized across plots to allow for easy comparison, but forcing high standardized volume values off the plots. Bone density is measured as mg/mm³ partial density of hydroxyapatite. Histogram values are standardized by total bone volume. Images illustrating relative density curves for all bones are available at www.getahead.psu.edu/ApertDenVol for interested readers.

Landmark-based morphometric analysis indicates that *Fgfr2*^{+/P253R} mice can be differentiated from *Fgfr2*^{+/+} at P0 by brachycephaly, mid-facial hypoplasia, an anteriorly displaced cranial base, as well as synostosis of the coronal, maxillary-zygomatic, and premax-maxillary sutures (Wang et al., 2010; Martínez-Abadías et al., 2010; Hill et al., 2013). The bones for which volume is most strongly influenced at E15.5–E16.5 and for which relative bone density is influenced across the prenatal period include bones of the face. Landmark

based measures suggest shorter linear scale of facial bones in *Fgfr2*^{+/P253R} mice at P0 (Wang et al., 2010; Martínez-Abadías et al., 2010; Hill et al., 2013) as well as reduced growth of the palate and face between E17.5 and P0 (Motch et al., 2012). However, we find that facial bones display similar (or higher) volumes at E17.5 and P0, indicating a lack of correlation between landmark based and volume based measures of bone scale. Overall, *Fgfr2*^{+/P253R} mice display thicker or squatter facial bones with reduced density at E17.5 and P0.

If a shift in the balance between osteoblast lineage proliferation and differentiation occurs as described above across all facial bones, this may explain the bone volume catch-up noted in our prenatal results. An increase in osteoblast differentiation at the expense of proliferation (and perhaps migration) may be directly responsible for the increased rate of ossification and the subsequent thicker morphology of many bones of the *Fgfr2*^{+/P253R} mice by E17.5 and P0. It is plausible that the quick increase in volume and thickening of maxillae and premaxillae, which start out smaller than normal at E16.5, may contribute to the overall morphology of midfacial hypoplasia. We also suggest that the thickening of these bones without adequate proliferation and subsequent migration of osteoblast precursors outward may cause the edges of the premaxilla and the maxilla to approach and touch, contributing to the premature fusion of the premax-maxillary suture.

Our results of significant early differences in total bone volume and relative density, followed by evidence of catch-up ossification before birth, highlight the importance of looking at the effect of the P253R mutation on osteoblast lineage activity across whole bones, rather than only focusing on the suture. In combination with landmark based linear measurements, bone volume and relative density provide a more complete picture of the effect of a mutation on gross skeletal phenotype and serve as a basis for hypotheses on changes in cellular mechanisms that underlie pathology.

Postnatal Effect

A second shift in the influence of the P253R mutation on bone volume growth occurs postnatally. Between P0 and P2, *Fgfr2*^{+/P253R} bone volumes increase slower than *Fgfr2*^{+/+} volumes, leaving several bones that were equal in size at P0, significantly smaller at P2. The postnatal reduction in bone volume growth in this sample is similar to the reduction noted in the *Fgfr2*^{+/Y394C} mouse model of Beare-Stevenson craniosynostosis syndrome between P0 and P8 (Percival et al., 2012). Many bones

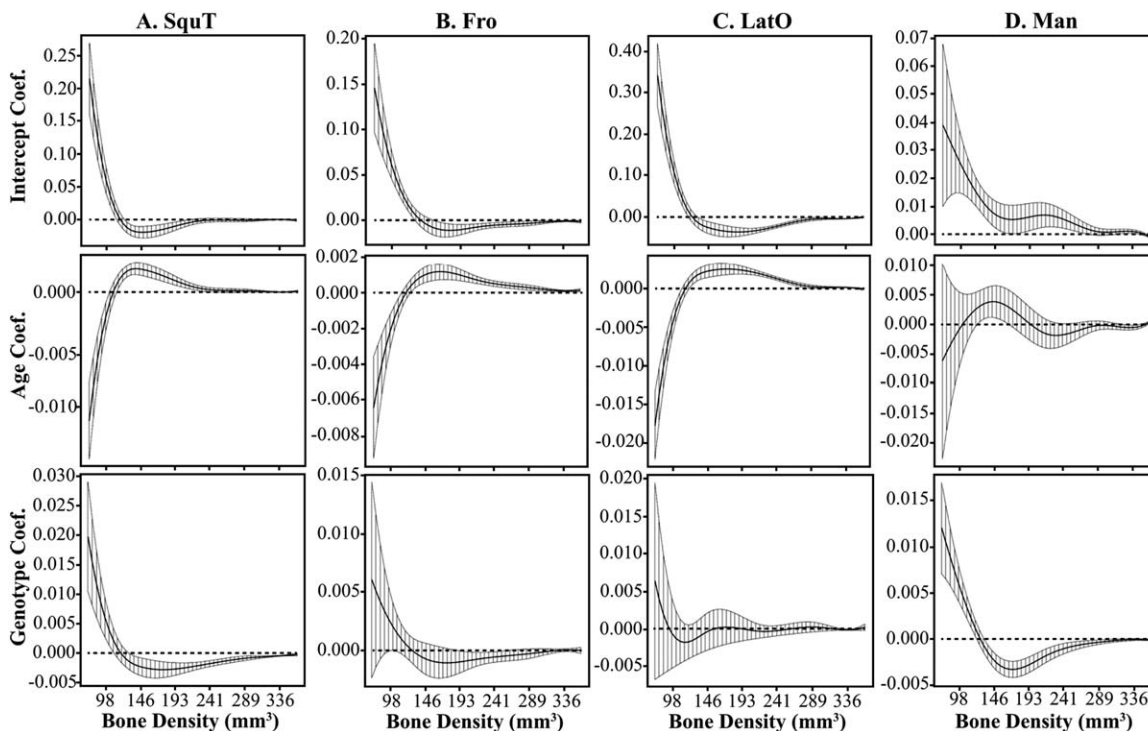


Fig. 6. The functional intercept, age, and genotype coefficients and 95% confidence intervals from prenatal multivariate regressions of relative bone density curves for four bones. The genotype coefficient illustrates how the $Fgfr2^{+/P253R}$ mice differ from unaffected littermates, independent of age. The y-axis differs for all plots. **A:** SquT displays a significant genotype effect between E15.5 and P0, which is opposite from the effect of increased age. The **(B)** Fro and **(C)** LatO do not display a significant genotype effect prenatally, but they do display a significant age effect over a wide range of density values. **D:** Man is among a few bones that displays a weakly significant age effect during the prenatal period. However, it displays a strong genotype effect. Bone abbreviations defined in Figure 2.

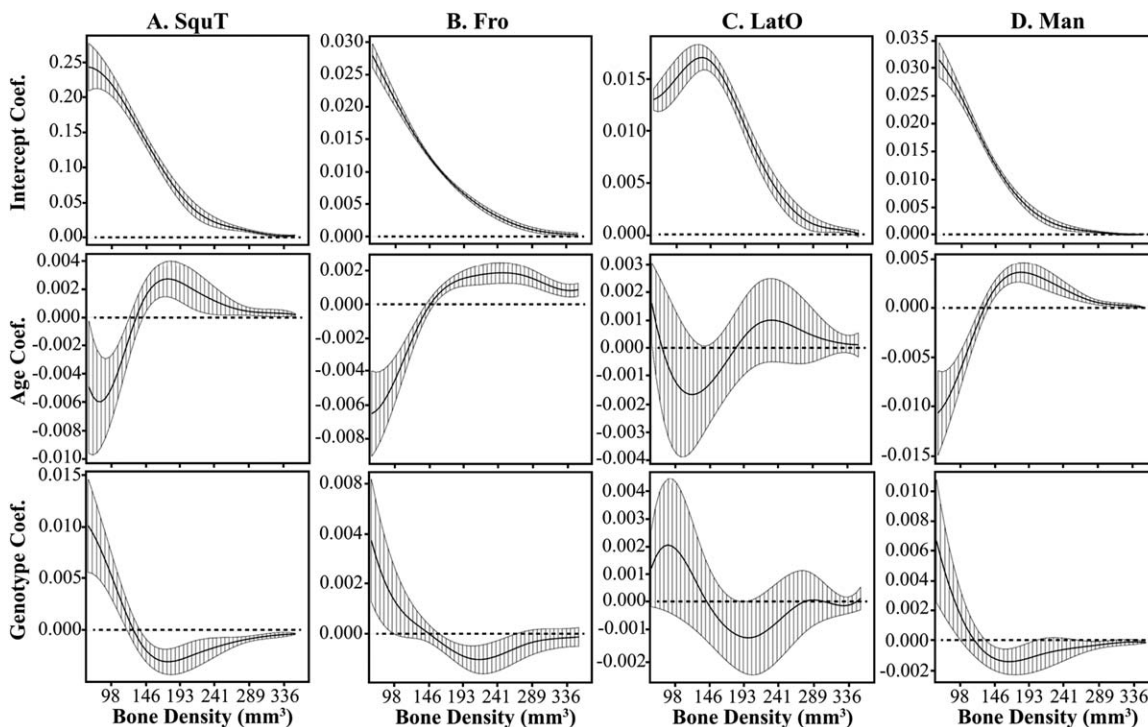


Fig. 7. The functional intercept, age, and genotype coefficients and 95% confidence intervals from postnatal multivariate regressions of relative bone density curves for four bones. The genotype coefficient illustrates how the $Fgfr2^{+/P253R}$ mice differ from unaffected littermates, independent of age. The y-axis differs for all plots. The **(A)** SquT and **(B)** Fro display significant genotype and age effects between P0 and P2, although the genotype coefficient is not significant over a wide range of bone density values. **C:** LatO does not display a significant genotype or age effect postnatally. **D:** Man displays a weakly significant effect of genotype and a strong effect of age during the postnatal period. Bone abbreviations defined in Figure 2.

that displayed lower relative bone density prenatally retain lower relative density postnatally, although it is unclear whether this is based on continued differences in bone maturation between the genotypes or is a carryover from the prenatal period.

The smaller volumes of many *Fgfr2*^{+/*P253R*} bones at P2 appear to match the great reduction in skull size noted between P0 and P2 in this model by previous morphometric analyses (Hill et al., 2013), including reduced size of the palate and rostral cranial base. In addition, the volumes of several neurocranial bones are reduced in P2 *Fgfr2*^{+/*P253R*} mice, suggesting that the previously noted increase in relative neurocranial height and width (Hill et al., 2013) is based on relatively wider fontanelles and sutures rather than increased ossification of the neurocranial elements. Such increased width is likely associated with wide midline calvarial defects, such as that noted in human infants with Apert syndrome (Cohen and Kreiborg, 1998).

Reduced postnatal *Fgfr2*^{+/*P253R*} bone volume would not be expected if increased osteoblast differentiation and bone expansion continued until P5 across all bones of the skull, as observed local to the leading ossification edges of the frontal and parietal bones making up the coronal suture (Wang et al., 2010). In fact, Par, which makes up one half of the coronal suture border, displays significantly lower volume at P2. These contrasting results illustrate differences in locally focused histological measures and estimates derived from whole bones. Assuming that a decrease in preosteoblastic cell proliferation and increase in differentiation occurs between E16.5 and E17.5, it is possible that postnatal populations of presumptive osteoblasts will be smaller within *Fgfr2*^{+/*P253R*} bones. A small progenitor cell population may limit the speed of bone growth and density increase via reduced potential for osteoblast differentiation and function. This hypothetical explanation for lower postnatal bone volumes for *Fgfr2*^{+/*P253R*} mice highlights the need for direct studies of bone cell activity in regions other than the coronal sutures of *Fgfr2* mutant mice if we are to understand the global effects of these mutations

on craniofacial development from the earliest embryonic periods onward. Given the increasing evidence that facial dysmorphology (Martínez-Abadías et al., 2010, 2013) and brain dysmorphology (Aldridge et al., 2010, Hill et al., 2013) occur as primary effects of known FGFR mutations, rather than secondary to calvarial suture fusion; studying the effect of Apert and other FGFR mutations on development across the head is a necessary step toward developing preventative treatments.

Summary

Using a refined version of our method to quantify bone volume and relative bone density (Percival et al., 2012), we quantify the “normal” pattern of early bone growth and maturation of individual mouse craniofacial bones and the influence of the P253R mutation on this pattern. Our results suggest that endochondral (group 1) and intramembranous cranial bones (groups 2 and 3) have fundamentally different patterns of bone maturation during initial osteogenesis. Endochondral bone density increases almost immediately following first ossification, while intramembranous bones retain a moderate or low level of bone density until the postnatal period, even as they significantly increase in volume. Although testing it is beyond the scope of this research, we hypothesize that the lower ‘normal’ levels of relative density increase in intramembranous bones stems from increased osteoblast lineage cell proliferation at the expense of differentiation during the earliest period of osteogenesis. In addition, further work on bone volume and relative density during the postnatal period will be required to determine whether the relative density of bones from all three groups becomes similar later in development.

Relative to our findings in unaffected littermates, mice carrying the *Fgfr2* P253R mutation show initially reduced volumes and relative density of many craniofacial bones during the earliest stages of ossification, including bones of the face that display some of the most serious dysmorphology associated with Apert syndrome. A change in the influence of this mutation on bone volume occurs

between E16.5 and E17.5, which could be associated with a previously noted decrease in osteoblast proliferation and increased differentiation at the coronal suture (Yin et al., 2008; Holmes et al., 2009; Wang et al., 2010). After bone volumes similar to those measured for unaffected littermates are noted across the skull at E17.5 and P0 in *Fgfr2*^{+/*P253R*} mice, the volumes and relative density of vault bones decrease between P0 and P2, as the overall relative linear scale of the *Fgfr2*^{+/*P253R*} skull is reduced and cranial dysmorphology increases. Early differences in the volume and relative density of facial bones associated with later suture fusion and midfacial hypoplasia suggest that the developmental changes underlying at least some Apert syndrome associated craniofacial dysmorphology occur during the earliest period of osteogenesis.

We found that facial bones previously shown by landmark based measures to be smaller in perinatal *Fgfr2*^{+/*P253R*} mice, had bone volumes similar to unaffected littermates at birth. This demonstrates that volumes of ossifying bones do not necessarily covary with landmark based measures of bone extent. Instead of relying on one type of phenotypic measure, the combination of complementary measures from landmark-based, volume, and relative density analyses provides a more complete picture of gross skeletal phenotype of individual craniofacial bones across the developing skull and illustrates the broader changes in individual bone development and maturation that are associated with craniofacial dysmorphology in Apert syndrome. We have suggested several testable hypotheses throughout our discussion about the cellular bases of noted differences in volume and density. Further work on the cellular activity in skull bones located distant to cranial vault and facial sutures are required to definitively connect the effects of this and other *Fgfr* mutations at the cellular level with noted differences in gross craniofacial phenotype.

ACKNOWLEDGEMENTS

Many thanks for the technical expertise and care by Tim Ryan and Tim Stecko at PSU CQI in producing the

μ CT images used in this study. Talia Pankratz completed valuable data collection on the P0 and P2 mice for this study. Thanks to Xueyan Zhou and Junghye Kim who organized and carried out a large part of the mouse breeding at Icahn School of Medicine at Mount Sinai and PSU, respectively. This work was supported in part by grants from the National Science Foundation to C.J.P. as well as to J.T.R. and collaborators and from the National Institute of Dental and Craniofacial Research and the American Recovery and Reinvestment act to J.T.R.

REFERENCES

- Aldridge K, Hill CA, Austin JR, Percival C, Martínez-Abadías N, Neuberger T, Wang Y, Jabs EW, Richtsmeier JT. 2010. Brain phenotypes in two FGFR2 mouse models for Apert syndrome. *Dev Dyn* 239:987–997.
- Beamer WG, Donahue LR, Rosen CJ, Baylink DJ. 1996. Genetic variability in adult bone density among inbred strains of mice. *Bone* 18:397–403.
- Beamer WG, Shultz KL, Donahue LR, Churchill GA, Sen S, Wergedal JR, Baylink DJ, Rosen CJ. 2001. Quantitative trait loci for femoral and lumbar vertebral bone mineral density in C57BL/6J and C3H/HeJ inbred strains of mice. *J Bone Miner Res* 16:1195–1206.
- Boehm B, Rautschka M, Quintana L, Raspopovic J, Jan Z, Sharpe J. 2011. A landmark-free morphometric staging system for the mouse limb bud. *Development* 138:1227–1234.
- Boughner JC, Wat S, Diewert VM, Young NM, Browder LW, Hallgrímsson B. 2008. Short-faced mice and developmental interactions between the brain and the face. *J Anat* 213:646–662.
- Bush JO, Jiang R. 2012. Palatogenesis: morphogenetic and molecular mechanisms of secondary palate development. *Development* 139:231–243.
- Cohen MM Jr, Kreiborg S. 1998. Suture formation, premature sutural fusion, and suture default zones in Apert syndrome. *Am J Med Genet Part A* 62:339–344.
- Cohen MM Jr, Maclean RE. 2000. Craniosynostosis: diagnosis, evaluation and management. 2nd ed. New York: Oxford University Press.
- Dixon MJ, Marazita ML, Beaty TH, Murray JC. 2011. Cleft lip and palate: understanding genetic and environmental influences. *Nat Rev Genet* 12:167–178.
- Du X, Weng T, Sun Q, Su N, Chen Z, Qi H, Jin M, Yin L, He Q, Chen L. 2010. Dynamic morphological changes in the skulls of mice mimicking human Apert syndrome resulting from gain-of-function mutation of FGFR2 (P253R). *J Anat* 217:97–105.
- Eames BF, Schneider RA. 2008. The genesis of cartilage size and shape during development and evolution. *Development* 135:3947–3958.
- Gritli-Linde A. 2008. The etiopathogenesis of cleft lip and cleft palate: usefulness and caveats of mouse models. *Curr Top Dev Biol* 84:37–138.
- Hallgrímsson B, Boughner JC, Turinsky A, Parsons TE, Logan C, Sensen CW. 2009. Geometric morphometrics and the study of development. In: Sensen CW, Hallgrímsson B, editors. *Advanced imaging in biology and medicine*. New York: Springer. p 319–336.
- Hill CA, Martínez-Abadías N, Motch SM, Austin JR, Wang Y, Jabs EW, Richtsmeier JT, Aldridge K. 2013. Postnatal brain and skull growth in an Apert syndrome mouse model. *Am J Med Genet Part A* 161:745–757.
- Hill CA, Reeves RH, Richtsmeier JT. 2007. Effects of aneuploidy on skull growth in a mouse model of Down syndrome. *J Anat* 210:394–405.
- Holmes G, Rothschild G, Roy UB, Deng CX, Mansukhani A, Basilico C. 2009. Early onset of craniosynostosis in an Apert mouse model reveals critical features of this pathology. *Dev Biol* 328:273–284.
- Kardong KV. 2012. *Vertebrates: comparative anatomy, function, evolution*. 6th ed. New York, NY: McGraw-Hill.
- Lana-Elola E, Rice R, Grigoriadis AE, Rice DPC. 2007. Cell fate specification during calvarial bone and suture development. *Dev Biol* 311:335–346.
- Martínez-Abadías N, Holmes G, Pankratz T, Wang Y, Zhou X, Jabs EW, Richtsmeier JT. 2013. From shape to cells: mouse models reveal mechanisms altering palate development in Apert syndrome. *Dis Model Mech* 6:768–779.
- Martínez-Abadías N, Percival C, Aldridge K, Hill C, Ryan T, Sirivunnabood S, Wang Y, Jabs E, Richtsmeier J. 2010. Beyond the closed suture in Apert mouse models: evidence of primary effects of FGFR2 signaling on facial shape at P0. *Dev Dyn* 239:3058–3071.
- Morriss-Kay GM, Wilkie AOM. 2005. Growth of the normal skull vault and its alteration in craniosynostosis: insights from human genetics and experimental studies. *J Anat* 207:637–653.
- Motch SM, Pankratz T, Percival CJ, Jabs EW, Richtsmeier JT. 2012. Development of the skull in Fgfr2+/P253R and Fgfr2+/S252W mouse models for Apert syndrome in late embryogenesis. Presentation at the 2012 Meeting of the Society for Craniofacial Genetics and Developmental Biology, San Francisco, California.
- Olson LE, Richtsmeier JT, Leszl J, Reeves RH. 2004. A chromosome 21 critical region does not cause specific Down syndrome phenotypes. *Science* 306:687–690.
- Passos-Bueno MR, Sertié AL, Jehée FS, Fanganiello R, Yeh E. 2008. Genetics of craniosynostosis: genes, syndromes, mutations and genotype-phenotype correlations. In: Rice DP, editor. *Craniofacial sutures: development, disease and treatment*. Vol. 12 Basel: Karger. p 107–143.
- Percival CJ, Wang Y, Zhou X, Jabs EW, Richtsmeier JT. 2012. The effect of a Beare-Stevenson syndrome Fgfr2 Y394C mutation on early craniofacial bone volume and relative bone mineral density in mice. *J Anat* 221:434–442.
- Percival CJ. 2013. The influence of angiogenesis on craniofacial development and evolution. Available from: <https://etda.libraries.psu.edu/paper/16838/>.
- Perlyn CA, DeLeon VB, Babbs C, Govier D, Burell L, Darvann T, Kreiborg S, Morriss-Kay G. 2006. The craniofacial phenotype of the Crozon mouse: analysis of a model for syndromic craniosynostosis using three-dimensional MicroCT. *Cleft Palate Craniofac J* 43:740–748.
- Ramsay JO, Hooker G, Graves S. 2009. *Functional data analysis with R and MATLAB*. New York, NY: Springer.
- Schmidt EJ, Parsons TE, Jamniczky HA, Gitelman J, Trpkov C, Boughner JC, Logan CC, Sensen CW, Hallgrímsson B. 2010. Micro-computed tomography-based phenotypic approaches in embryology: procedural artifacts on assessments of embryonic craniofacial growth and development. *BMC Dev Biol* 10:1–14.
- Wang Y, Sun M, Uhlhorn VL, Zhou X, Peter I, Martínez-Abadías N, Hill CA, Percival C, Richtsmeier JT, Huso DL, Jabs EW. 2010. Activation of p38 MAPK pathway in the skull abnormalities of Apert syndrome Fgfr2+/P253R mice. *BMC Dev Biol* 10:22.
- Yin L, Du X, Li C, Xu X, Chen Z, Su N, Zhao L, Qi H, Li F, Xue J. 2008. A Pro253Arg mutation in fibroblast growth factor receptor 2 (Fgfr2) causes skeleton malformation mimicking human Apert syndrome by affecting both chondrogenesis and osteogenesis. *Bone* 42:631–643.
- Yoshida T, Vivatbutsi P, Morriss-Kay G, Saga Y, Iseki S. 2008. Cell lineage in mammalian craniofacial mesenchyme. *Mech Dev* 125:797–808.